Article:
Musonda, E and Hunter, IC (2015) Exact Design of a New Class of Generalized Chebyshev Low-Pass Filters Using Coupled Line/Stub Sections. IEEE Transactions on Microwave Theory and Techniques, 63 (12). pp. 4355-4365. ISSN 0018-9480

https://doi.org/10.1109/TMTT.2015.2492969

Exact Design of a New Class of Generalised Chebyshev Low-pass Filters Using Coupled Line/Stub Sections

Evaristo Musonda, Student Member, IEEE, Ian C. Hunter, Fellow, IEEE

Abstract— A method for the design of a new class of distributed low-pass filters enables exact realization of the series short circuited transmission lines which are normally approximated via unit elements in other filter realisations. The filters are based upon basic sections using a pair of coupled lines which are terminated at one end in open-circuited stubs. The approach enables realisation of transmission zeros at the quarter –wave frequency hence giving improved stopband performance. A complete design theory starting from a distributed generalised Chebyshev low-pass prototype filter is presented. A design example demonstrates excellent performance in good agreement with theory.

Index Terms—Distributed low-pass filters, Generalized Chebyshev, Meander Line, Selectivity, TEM

I. Introduction

Low-pass filters are often needed in microwave systems to 'clean up' spurious responses in the stopband of coaxial and dielectric resonator filters. The most important driving factors are compact size, sharp roll-off and wide stopband. Some of the recent works have addressed some of these problems [1, 2]. Although it is relatively easy to obtain theoretical circuit models, the challenge in practical low-pass filters lies in achieving good approximation using real transmission line components.

There exist many realisations for low-pass filters. One popular type is the stepped impedance low-pass filter consisting of interconnections of commensurate lengths of transmission lines of alternating low and high impedance [3]. This type of filter has low selectivity for a given network order because the transmission zeros are all at infinity on the real axis in the complex plane.

In order to increase selectivity, transmission zeros may be placed at finite frequencies using distributed generalised Chebyshev prototype filters [4]. The problem is that there is no direct realisation of the series short circuited stubs associated with this low-pass prototype filter. In the existing physical realisation [5] the series short circuited stubs are approximated by short lengths of high impedance transmission line (forcing those transmission zeros at a quarter-wave frequency to move to infinity on the real axis), while the shunt series foster is realised exactly as an open circuited stub of double unit length. The approximation involved results in relatively poor stopband rejection.

As an expansion to the work described in [6], this paper presents two solutions in which the series short circuited stubs are exactly realised within the equivalent circuit of the filter. In section II, the synthesis techniques for the two physical realisations have been developed. In the previous paper, only the equivalent circuit for the second low-pass filter physical realisation was known and the element values were obtained via optimisation in a circuit simulator. In this revised and expanded paper, the synthesis is developed and presented together with the required canonical low-pass circuit forms and corresponding transmission zeros that the transfer functions may realise. The procedure for different low-pass filter degrees is included with the required circuit transformations which was a significant piece of work. Design examples are included to illustrate the synthesis technique.

II. Design Theory

In Fig. 1, the general physical layout is given for the proposed method. The structure consists of a middle section of high impedance coupled lines terminated at every alternate end in a low impedance open-circuit stub forming a 'meander-like' structure as in Fig. 1. All the transmission lines are of commensurate length. Grounded decoupling walls must be utilised to eliminate coupling between the open-circuited stubs.

In this work it is shown how a general Chebyshev transfer function may be used to implement two alternative realisations arising from Fig. 1. via a series of derived circuit transformations and one of the earlier transformation derived by Sato in Table I of [7]. The synthesis of distributed low-pass filter networks is based on work done in [8]. Fig 2 shows the derived equivalent circuit transformations and the required admittance relationships. The next two sections describe how

Manuscript received June 24, 2015; revised September 15, 2015; accepted October 11, 2015. This work was supported in part by the Beit Trust, Surrey, UK, the University of Leeds, Leeds, UK, RS Microwave Inc., Butler, NJ, USA, Radio Design Limited, Shipley, West Yorkshire, UK and The Royal Academy of Engineering, London, UK. This paper is an expanded version from the IEEE MTT-S International Microwave Symposium, Phoenix, AZ, USA, 17-22 May 2015.

The authors are with the Institute of Microwave and Photonics, School of Electronic and Electrical Engineering, University of Leeds, LS2 9JT Leeds, UK (e-mail: el11em@leeds.ac.uk).

these transformations were used to derive the equivalent circuit for the two possible physical realisations from their canonical low-pass filter derivatives.

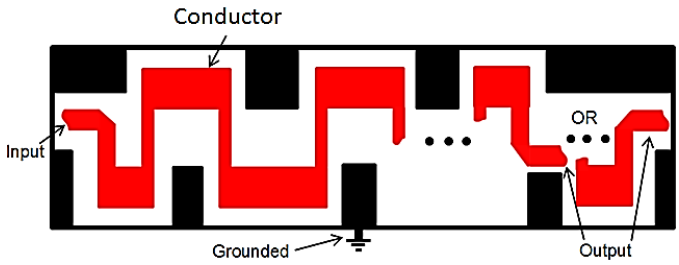

(a)

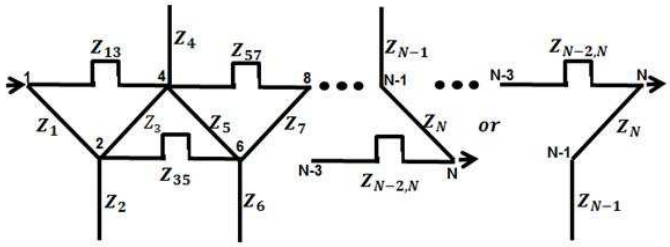

(b)

Fig. 1. Proposed layout of meander-like low-pass filter (a) composed of a section of high impedance parallel coupled lines short circuited by a low impedance open circuited stub at alternate ends (b) graphical line equivalent circuit

Transformation I $y_0 = y_2(y_1 + y_3 + y_4) + y_3(y_1 + y_4)$ $y_a = \frac{y_1 y_2 y_3}{y_0}$ $y_b = \frac{{y_3}^2(y_1 + y_2 + y_4)}{y_0}$ $y_c = \frac{y_2 y_3 y_4}{y_0}$ $y_{ab} = \frac{y_1 y_4 (y_2 + y_3)}{y_0}$	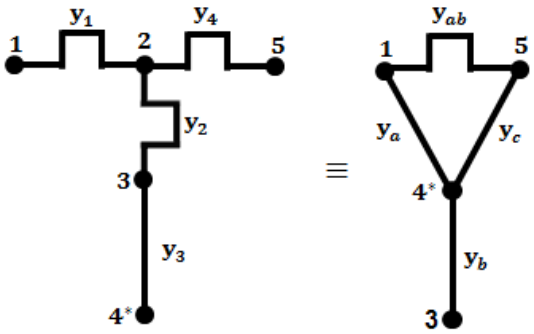
Transformation II $y_0 = y_1 + y_2 + y_3$ $y_a = \frac{y_1 y_2}{y_0}$ $y_c = \frac{y_2 y_3}{y_0}$ $y_b = \frac{{y_2}^2}{y_0}$ $y_{ab} = \frac{y_1 y_3}{y_0}$	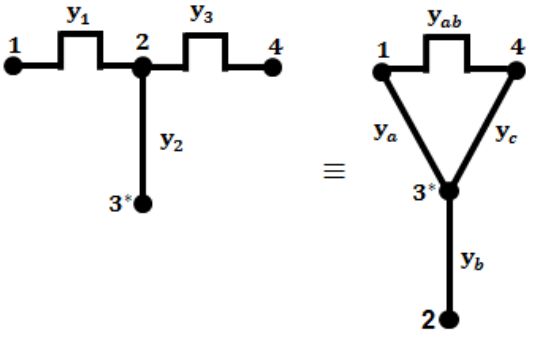
Transformation III Choose y_b $y_a = y_1 + y_2 - y_b$ $y_{ab} = \frac{y_a(y_2 - y_b)}{y_1}$	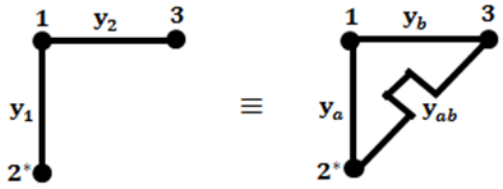

Transformation IV

$$A = \frac{4{y_1}^2 y_4(y_3 + y_4 + y_5)}{{y_2}^2 y_3 y_5}$$

$$B = \frac{4y_1 y_4(2y_3 y_5 + 2y_4 y_5 + {y_5}^2)}{y_2 y_3 y_5}$$

$$C = \frac{y_5({y_3}^2 + 4{y_4}^2 + 4y_3 y_4)}{y_3}$$

$$y_a = \frac{-B \pm \sqrt{B - 4AC}}{2A}$$

$$y_b = \sqrt{y_a\left(y_5 - \frac{y_a y_1}{y_2}\right)}$$

$$y_c = \frac{y_3 y_5 y_a}{2y_4 y_b}$$

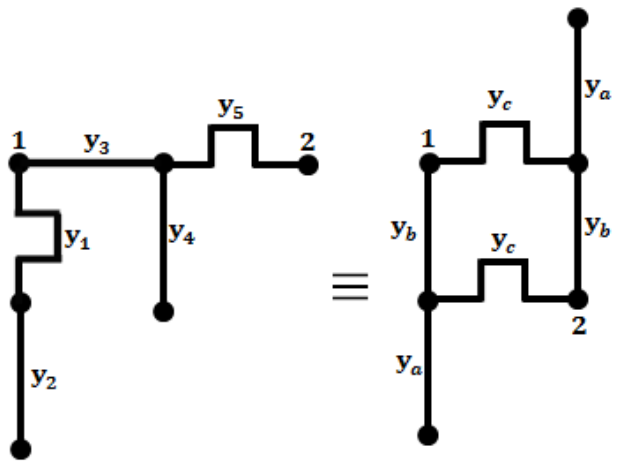

Transformation V

$$y_{ab} = y_{bc}$$

$$y_b = y_2 + 2\sqrt{y_2 y_{12}}$$

$$y_{ab} = 2y_{12} + \sqrt{y_2 y_{12}}$$

$$y_o = y_b + 2y_{ab}$$

$$y_a = y_1 - \frac{y_b y_{ab}}{y_o}$$

$$y_c = y_3 - \frac{y_b y_{ab}}{y_o}$$

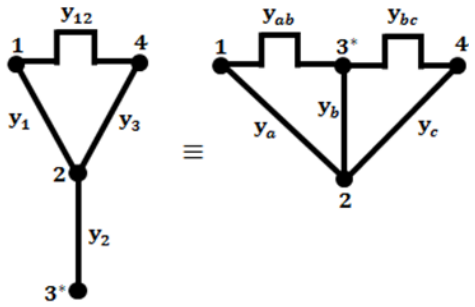

Fig. 2 Derived equivalent circuit transformations (*May be a hanging node)

A. Physical Realisation I

The first physical realisation realises the equivalent circuit for the general Chebyshev distributed network given in Fig. 3. By using the synthesis technique given in [8], the network of Fig. 3 may be synthesized directly in distributed domain from an N^{th} (N odd) -degree Chebyshev transfer function with $(N-1)/2$ pairs of symmetrically located transmission zeros ($\pm\theta_z$) and a single transmission zero at a quarter-wave frequency ($\theta_z = \pm 90^o$).

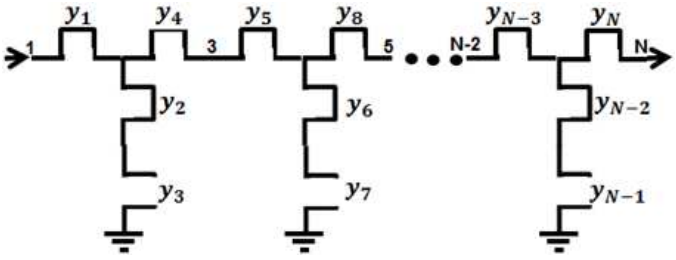

Fig. 3 Generalised Chebyshev distributed low-pass prototype

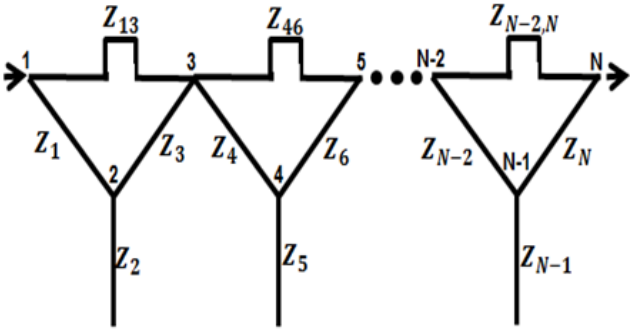

Fig. 4 Graphical representation of the equivalent circuit of Fig. 3 after transformation of the 3rd -degree basic sections

In this work N-N_{FTZ}-N_{90^o} simply refers to an N^{th} -degree low-pass filter with N_{FTZ} number of transmission zeros at some general frequency in the complex plane, N_{90^o} number of transmission zeros at quarter-wave frequency (i.e. $\theta_z = \pm 90^o$) and $(N - N_{FTZ} - N_{90^o})$ number of real axis half transmission zero pair at infinity (i.e. $\theta_z = \pm j\infty$). Where N_{FTZ} exists, these transmission zeros may either be symmetrically pure imaginary frequency pairs (i.e. $\theta_z = \pm\theta_\omega$), or in general paraconjugated pairs on the complex plane (i.e. $\theta_z = \theta_\omega \pm j\theta_\sigma$), such that N_{FTZ} is always even. Therefore, in general the distributed network of Fig. 3 is of the form N-$(N-1)/2$-1.

Using circuit transformation I on each of the 3rd -degree section, Fig. 3 may be transformed into Fig. 4. It is then clear

from Fig. 4 that each of the 3rd -degree section is just the equivalent circuit of a pair of two parallel coupled lines with one end terminated in an open circuited stub as depicted in Fig. 5. The overall network after the transformation is illustrated in Fig. 6. This is equivalent to Fig. 1(a) but with every second coupling between the parallel coupled lines section removed (i.e. couplings Z_{35}, Z_{79}, … removed in Fig. 1(b)), such that the structure is composed of cascaded 3rd -degree basic sections of Fig. 5 as shown in Fig. 6.

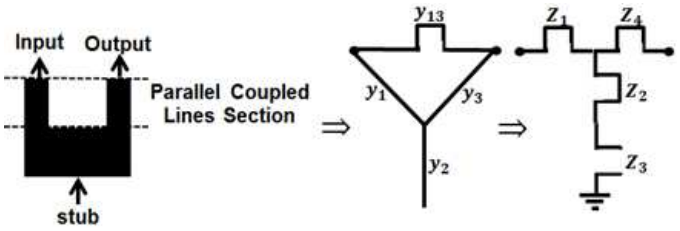

Fig. 5 A basic section containing a pair of coupled line and a stub and its equivalent circuits

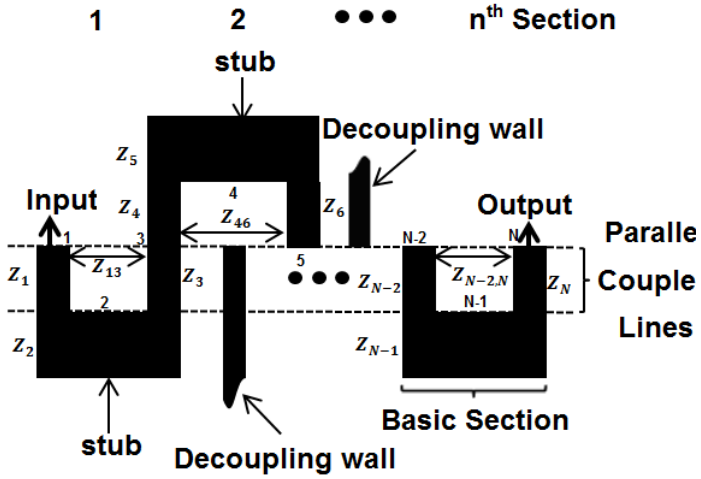

Fig. 6 Physical layout for generalised Chebyshev distributed low-pass prototype filter of physical realisation I

1) Design Example

A 7th -degree low-pass filter was designed using the techniques described above with cutoff frequency at 1 GHz, 20 dB minimum passband return loss with pairs of finite transmission zeros at $\theta_z = \pm 54.44^o$, $\pm 43.00^o$ and $\pm 54.44^o$ (2.18, 1.72 and 2.18 GHz) and a single quarter-wave transmission zero ($\theta_z = \pm 90^o$) and electrical length at the cutoff frequency, $\theta_c = 25^o$.The element values are shown in Table I corresponding to the circuit of Fig. 3 where symmetry is assumed for the element values. Using the circuit transformation I, the circuit was transformed to the final form of Fig. 4 with the element values shown in Table II. All the element values are clearly realizable. Fig. 7 shows the circuit simulation of the design example.

TABLE I
7TH -DEGREE LOW-PASS FILTER SYNTHESISED ADMITTANCE VALUES ($\mho$)

Section 1	Section II	Section III
$y_1 = 0.4983$	$y_5 = 0.5830$	$y_9 = 0.4983$
$y_2 = 5.5807$	$y_6 = 2.5671$	$y_{10} = 5.5807$
$y_3 = 2.8517$	$y_7 = 2.9514$	$y_{11} = 2.8517$
$y_4 = 0.4983$	$y_8 = 0.5830$	$y_{12} = 0.4983$

TABLE II
7TH -DEGREE LOW-PASS FILTER IMPEDANCE VALUES (Ω) AFTER TRANSFORMATION II (A)-(C) IN 50 Ω SYSTEM

Section 1&3	$Z_1 = 153.3$ $Z_2 = 22.73$ $Z_3 = 153.3$	$Z_{13} = 580.7$
Section 2	$Z_4 = 158.6$ $Z_5 = 21.54$ $Z_6 = 158.6$	$Z_{46} = 373.5$

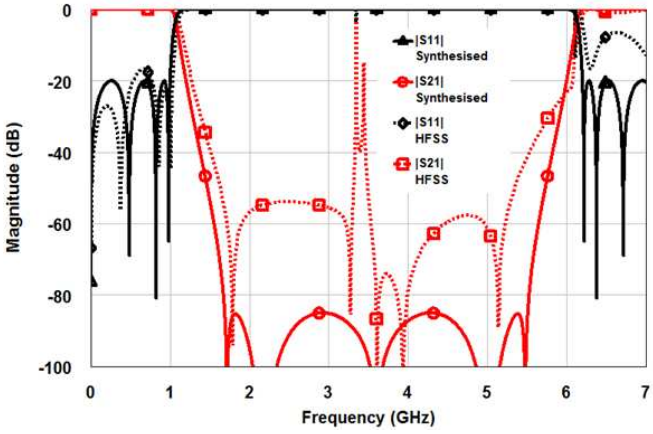

Fig. 7 Circuit and HFSS simulation response for example I

In this realisation I, $\theta_c = 25^o$ is approaching practical limits for realisable element values. Reducing the electrical length at the cutoff frequency further causes the impedance values of the high and low impedance lines to become unrealizably high and low respectively. However, in reality the practical stopband bandwidth is perturbed due to high order modes and spurious couplings between the basic sections as shown by the HFSS simulation in Fig. 7 with small resonance peaks around $\theta = 90^o$. The decoupling walls do not give exact circuit realisation for realisation I. In the second physical realisation, however, some of the couplings are allowed between basic sections.

B. Physical Realisation II – *'Meander-like'* Low-pass Filter

A more general realisation is achieved by using the layout of Fig. 1. The only difference with the previous physical realisation I is that, in the general case, physical realisation II, all the couplings between high impedance coupled lines of Fig. 1 are allowed. The structure is built from the basic 3rd -

degree section of Fig. 5 by adding a parallel line to the parallel coupled lines section and an open circuited stub at one end to form an interconnect each time to increase the network degree by 2.

The stripline layout for physical realisation II is given in Fig. 8 and its derived equivalent circuit is shown below in Fig. 9 with the unit element impedance values named sequentially from input to output. This realisation is optimal since an N^{th} -degree filter requires N commensurate length transmission lines. At the quarter-wave frequency, all the series short circuited stubs become open circuited while all the open circuited stubs become short circuited so that the alternate ends of the parallel coupled lines are shorted to ground. Thus the meander-like low-pass filter of Fig. 8 has at least one transmission zero at the quarter-wave frequency. The other transmission zero pairs may exist at infinity on the real axis or as symmetrical pure imaginary frequency pair or in general as paraconjugated pairs on the complex plane due to multipath in the structure.

It is now shown how the meander-like low-pass filter network of Fig. 8 and Fig. 9 may be synthesized from suitable low-pass filter networks and then using appropriate circuit transformation to transform the canonical low-pass filter network forms to a meander-like low-pass filter. The canonical low-pass filter network forms were obtained by the synthesis method in [8] and then applying cascaded synthesis. The 3rd, 5th, 7th and 9th -degree meander-like low-pass filter are examined next as depicted in Fig. 10.

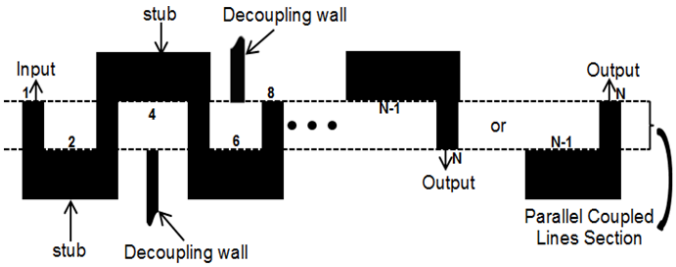

Fig. 8 Physical layout of the striplines for the general meander-like low-pass filter with allowed coupling between parallel lines of the adjacent basic sections.

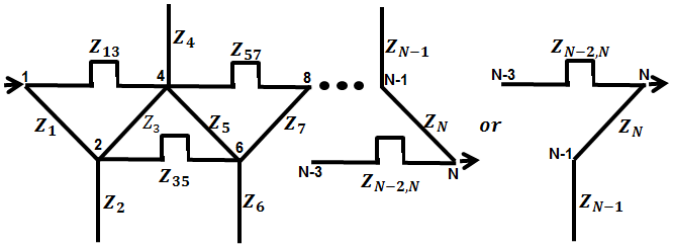

Fig. 9 Graphical representation of the equivalent circuit of Fig. 8 for a meander-like low-pass filter

The 3rd -degree filter is simply a trivial case corresponding to circuit transformation I as shown in Fig. 10 (I). In this case a 3-0-3 or 3-2-1 low-pass filter may be realised.

I N=3 (3-2-1)	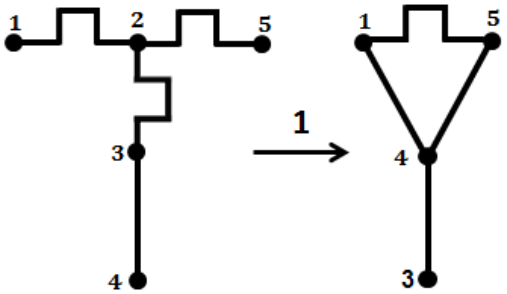
II N=5 (5-0-4)	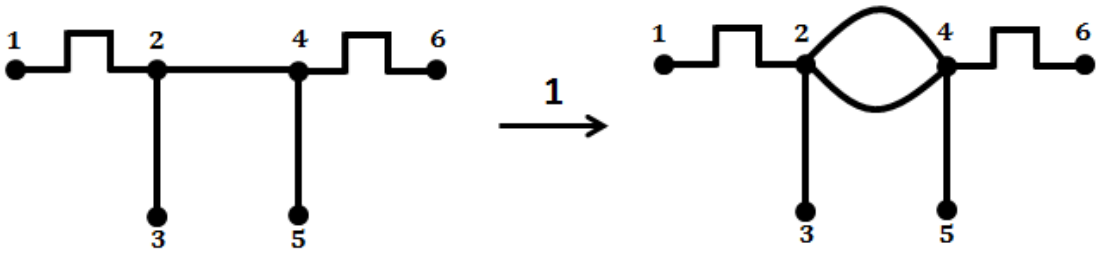

II N=5 (5-0-4)	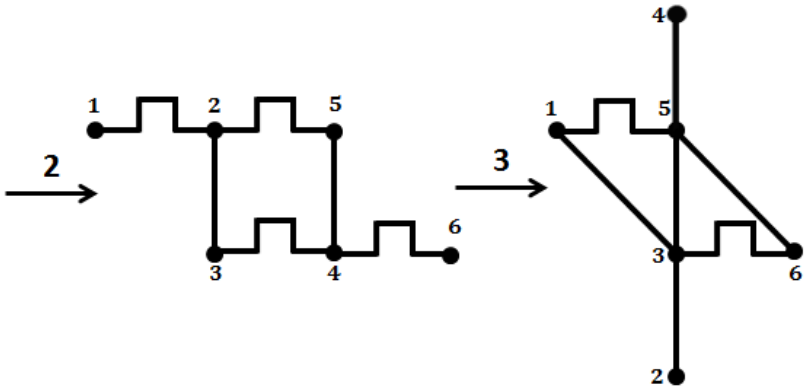
III N=5 (5-2-2) Asymmetrical	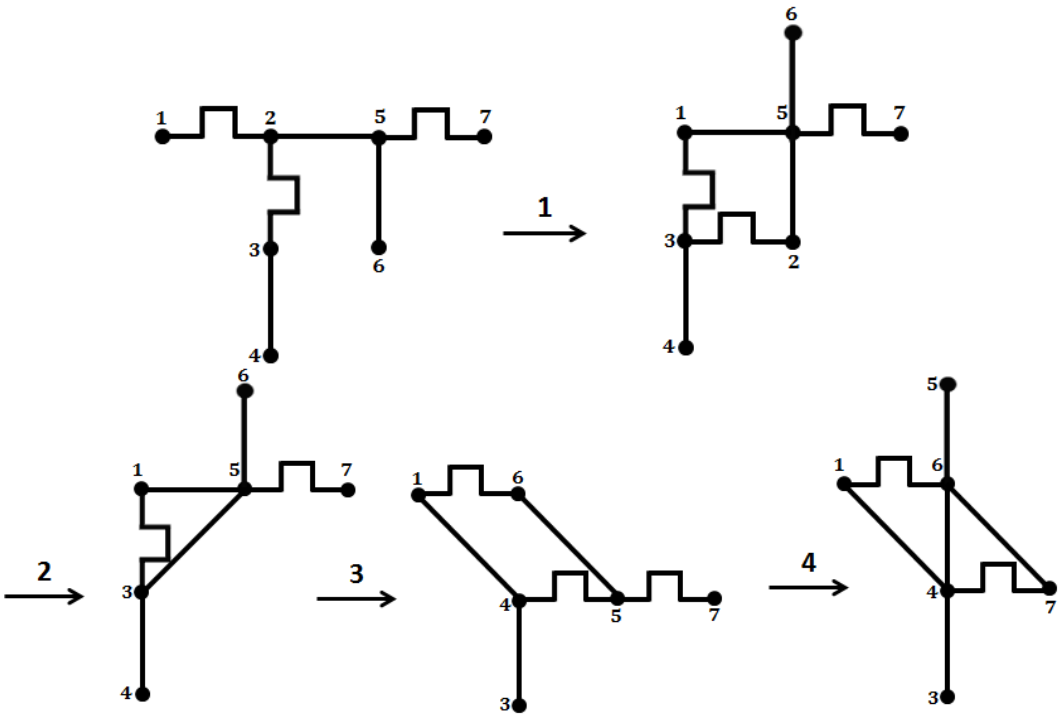
IV N=5 (5-2-2) Symmetrical	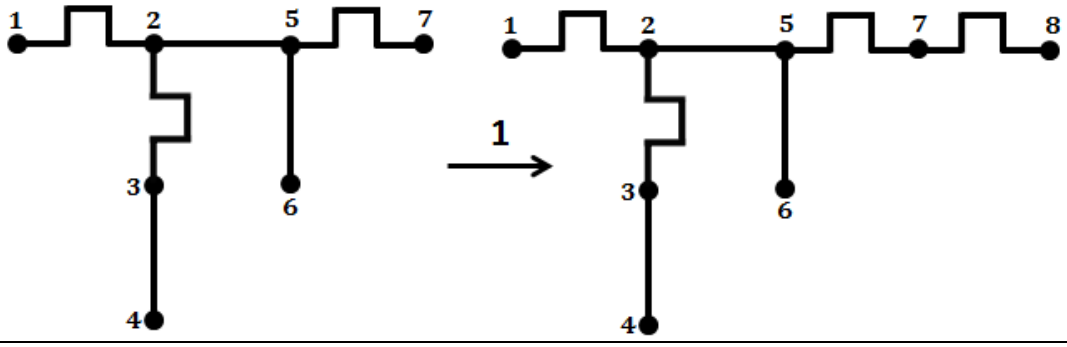

IV N=5 (5-2-2) Symmetrical	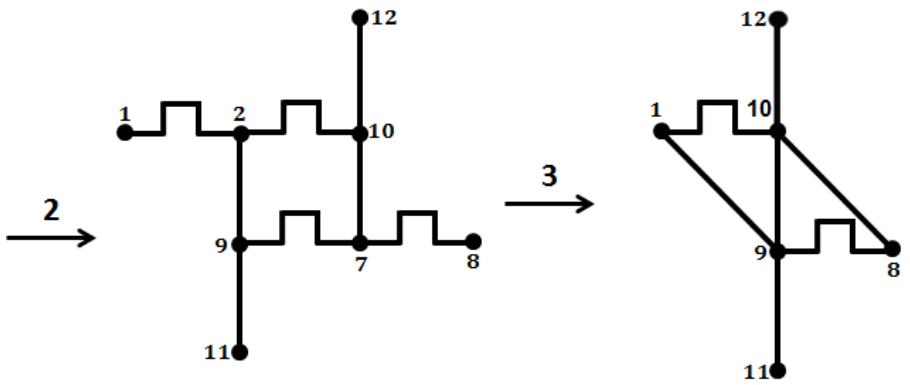
V N=7 (7-2-5)	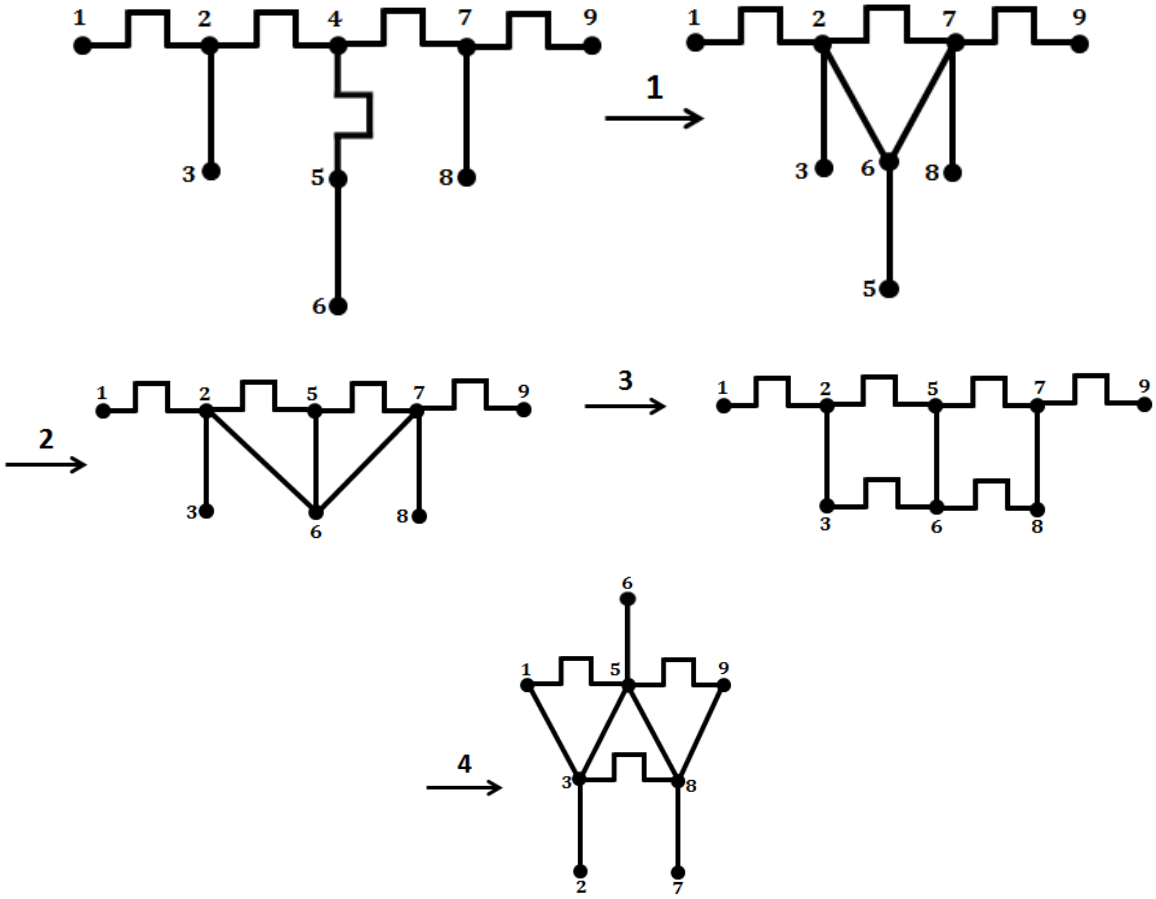
VI N=9 (9-0-8)	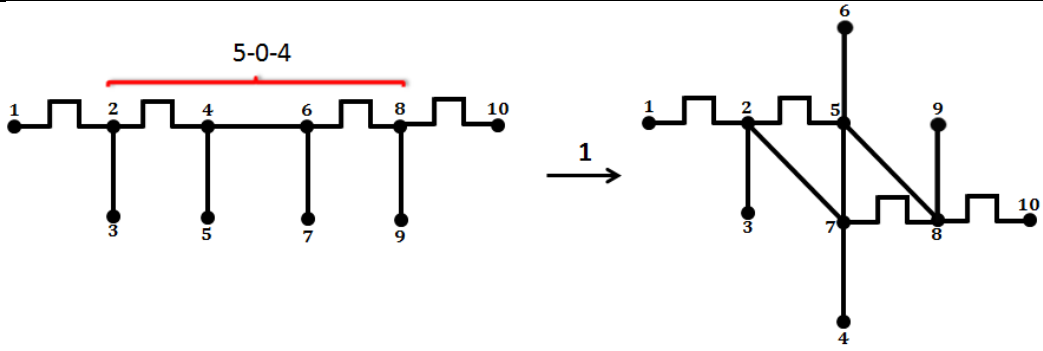

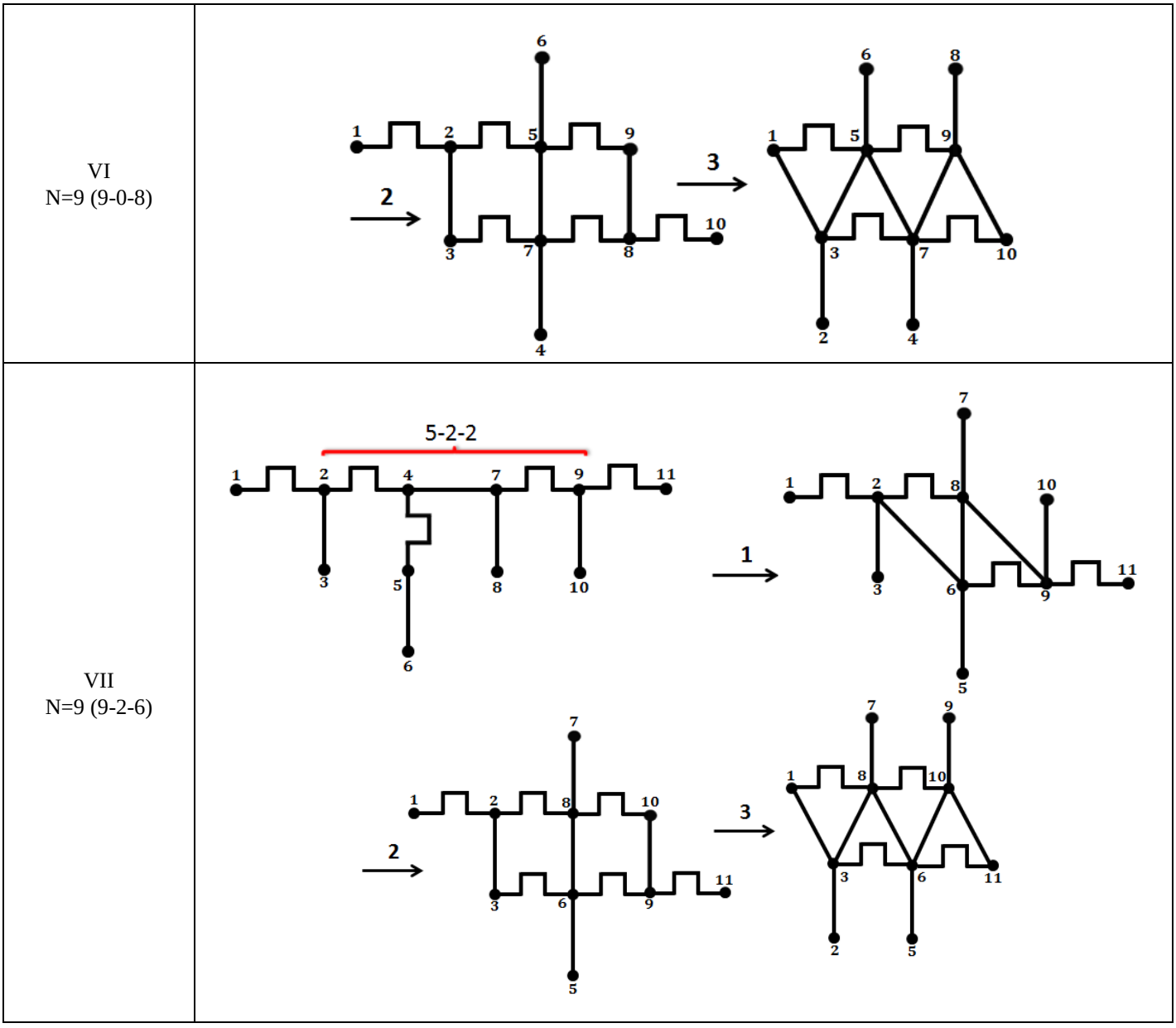

Fig. 10 Derived network transformation for $N = 3,5,7$ and 9 meander-like low-pass filters

There are two possible cases for 5th -degree filter, namely 5-0-4 and 5-2-2 low-pass filter. For the first case of Fig. 10 (II), a 5-0-4 low-pass filter has a single real axis half transmission zero pair at infinity ($\theta_z = \pm j\infty$) and four transmission zeros are at a quarter-wave frequency ($\theta_z = \pm 90^o$). Beginning with the canonical network form, step 1 is to split the transmission lines into two equal parts between port 2 and 4. In step 2, transformation III is carried out on each of the branch 3,2,4 and 2,4,5 respectively. Finally in step 3, two separate transformations II are carried out on each of the three port subnetworks of 1,3,5 and 3,5,6 to derive the final equivalent circuit as illustrated in Fig. 10 (II).

The second meander-like low-pass filters, the 5-2-2 low-pass filter in Fig. 10 (III and IV), have a single pair of symmetrical finite frequency transmission zeros ($\theta_z = \pm\theta_\omega$), a single real axis half transmission zero pair at infinity ($\theta_z = \pm j\infty$) and two transmission zeros at the quarter-wave frequency ($\theta_z = \pm 90^o$). For an asymmetrical 5-2-2 case of Fig. 10 (III), step 1 utilises Sato's transformation (Table I of [7]) to eliminate branch 1,2 and in turn creates branch 1,3 and 1,5. In Step 2, Sato's transformation is used again to eliminate branch 2,3 and creates branch 3,5. In step 3, transformation III is applied on branch 1,5,6 and two sequential transformations III are applied on branch 1,3,5. The final equivalent circuit is obtained by application of transformation II on a three port subnetwork of 4,6,7 as illustrated in Fig. 10 (III).

For symmetrical 5-2-2 low-pass filter of Fig. 10 (IV), step 1 splits the inductor between node 5 and 7 such that the admittances of the outermost inductors in branch 1,2 and 7,8 are identical. In step 2, transformation IV is carried out on the

two port network between node 2 and 7 and finally two separate transformations II are carried out on three port subnetworks 1,9,10 and 9,8,10 respectively to obtain the final symmetrical form as illustrated in Fig. 10 (IV). Note that a negative sign on y_a in transformation IV should be taken for realizable impedance values.

For a 7th -degree filter, one possible realisation derived, is a 7-2-5 low-pass filter of Fig. 10 (V) with a single pair of symmetrical finite frequency transmission zero pair ($\theta_z = \pm\theta_\omega$) and all the remaining five transmission zeros at the quarter-wave frequency ($\theta_z = \pm 90^o$) which is now illustrated. From the canonical low-pass filter form, transformation I is applied on the two port network between node 2 and 7 in step 1. This is followed by transformation V again on the same two port network between node 2 and 7 in step 2. Then in step 3, two separate transformation III are applied on branch 3,2,6 and 8,7,9 and finally in step 4, three separate transformation II are applied on three port subnetworks of 1,3,5, 3,5,8 and 5,8,9 respectively to obtained the final form of the meander-like low-pass filter of Fig. 10 (V).

For a 9th -degree filter, two derivative low-pass filter networks were examined whose core subnetworks were derived from a 5th -degree network discussed above.

The first one is a 9-0-8 filter, with a single real axis half transmission zero pair at infinity ($\theta_z = \pm j\infty$) and all remaining eight transmission zeros at a quarter-wavelength frequency ($\theta_z = \pm 90^o$). Beginning with the canonical low-pass filter in Fig 10 (VI) in step 1, a two port network between node 2 and 8 is replaced by a derived circuit for a 5-0-4 circuit as explained above (Fig. 10 (II)). Then in step 2, two separate transformations III are applied to branch 3,2,7 and 5,8,9. This is followed by two separate transformations II which are applied on three port subnetworks of 1,3,5 and 7,9,10 respectively to give the final equivalent circuit as illustrated in Fig. 10 (VI).

The second 9th -degree low-pass filter is a 9-2-6 low-pass filter with a single symmetrical pair of finite frequency transmission zeros ($\theta_z = \pm\theta_\omega$), a single real axis half transmission zero pair at infinity ($\theta_z = \pm j\infty$) and all remaining six transmission zeros at a quarter-wave frequency ($\theta_z = \pm 90^o$). Beginning with the canonical low-pass filter form in Fig 10 (VII) in step 1, a two port network between node 2 and 9 is replaced by a derived circuit for a 5-2-2 circuit as explained above (Fig. 10(III or IV)). Then in step 2, two separate transformations III are applied to branch 3,2,6 and 8,9,10 respectively. This is followed by two separate transformations II which are applied on three port subnetworks of 1,3,8 and 6,10,11 respectively to give the final equivalent circuit shown in Fig. 10 (VII). Note that a positive sign on y_a in transformation IV should be taken for realizable impedance values.

Multiple solutions do exist depending on the transformations used. Impedance levels are within positive realisable values as long as the electrical length at the cutoff is chosen to be around $\theta_c = \pm 45^o$ as the two examples will show. Moving further away form $\theta_c = \pm 45^o$ either direction tend to lead to extreme element's impedance values some of which may assume negative values arising from the formulae used in some of the cases of Fig. 2. As its canonical circuit form, the meander-like low-pass filter is relatively unaffected by small changes in the impedances values because it requires an optimal number of elements (N). Thus small mismatch in the impedance values only slightly degrades the passband return loss.

1) Design Example I

A 7th -degree (7-2-5) meander-like low-pass was designed with a symmetrical pair of finite frequency transmission zero at $\theta_z = \pm 65^o$(1.625 GHz) and five transmission zeros at a quarter-wave frequency ($\theta_Z = \pm 90^o$), 20 dB minimum passband return loss and electrical length of $\theta_c = \pm 40^o$at cutoff frequency of 1 GHz. The synthesised element values for the canonical low-pass filter is shown in Table III (assuming symmetry with impedance values assigned sequentially from left to right of Fig. 10 (V)). Then using the technique as explained in section II (B) and Fig. 10 (V) by a sequence of circuit transformations, the meander-like element values were obtained as shown in Table IV. The circuit simulation shown in Fig. 11 validates the synthesis process.

TABLE III
7TH -DEGREE CANONICAL LOW-PASS FILTER IMPEDANCE VALUES (Ω)

$Z1 = 60.2932$	$Z4 = 6.2196$
$Z2 = 29.1279$	$Z5 = 28.6033$
$Z3 = 110.2028$	

TABLE IV
7TH -DEGREE MEANDER-LIKE LOW-PASS FILTER IMPEDANCE VALUES (Ω)

$Z1 = 108.2319$	$Z13 = 362.2136$
$Z2 = 53.7139$	$Z35 = 44439.57$
$Z3 = 215.9667$	
$Z4 = 25.8734$	

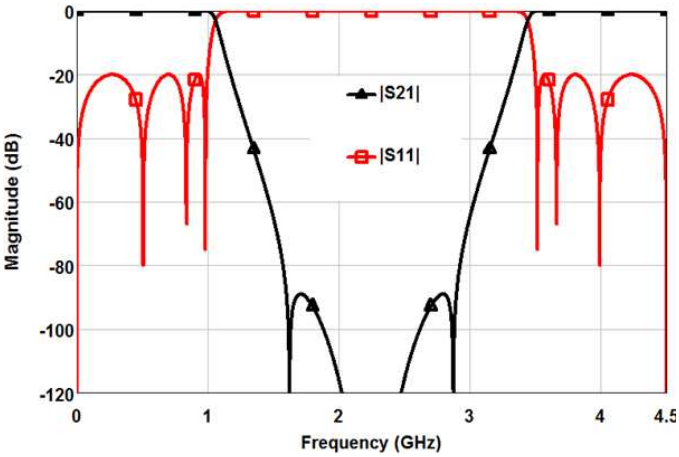

Fig. 11 Circuit simulation of a 7-2-5 meander-like low-pass filter in example II B (1)

2) Design Example II

An experimental 9th -degree meander-like low-pass filter was designed with cutoff frequency at 1 GHz, 20 dB minimum return loss and $\theta_c = \pm 45^o$. The stopband insertion loss was defined to be above 70 dB between 1.3 GHz and 2.7 GHz and this was achieved by placing a symmetrical transmission zero pair at $\theta_z = \pm 58.23^o$(1.294 GHz), a single real axis half transmission zero pair at infinity ($\theta_z = \pm j\infty$) and six transmission zeros at quarter-wave frequency ($\theta_z = \pm 90^o$) yielding a 9-2-6 low-pass filter of fig. 10 (VII). The synthesised element values for the canonical 9th -degree low-pass filter are shown in Table V. These values were transformed to the meander-like circuit with the element values shown in Table VI.

TABLE V
SYNTHESISED 9TH -DEGREE CANONICAL LOW-PASS FILTER IMPEDANCE VALUES (Ω)

$Z1 = 51.3388$	$Z6 = 114.8003$
$Z2 = 34.1469$	$Z7 = 30.5252$
$Z3 = 86.4301$	$Z8 = 99.4671$
$Z4 = 15.2258$	$Z9 = 34.1469$
$Z5 = 39.6987$	$Z10 = 51.3388$

TABLE VI
SYNTHESISED 9TH -DEGREE MEANDER-LIKE LOW-PASS FILTER IMPEDANCE VALUES (Ω)

$Z1 = 101.2065$	$Z13 = 317.8744$
$Z2 = 66.08394$	$Z35 = 1798.938$
$Z3 = 207.5597$	
$Z4 = 34.02597$	
$Z5 = 147.2685$	

TABLE VII
9TH -DEGREE LOW-PASS FILTER OPTIMISED DIMENSIONS (MM)

$w1 = 9.04$	$sw1 = 12.5$	$s12 = 6.75$	$dL1 = 2.5$
$w2 = 1.85$	$sw2 = 3.00$	$s23 = 23.25$	$dL2 = 8.5$
$w3 = 2.33$	$sw3 = 7.25$	$b = 25$	$dL3 = 6.5$
$w4 = 17.64$	$sw4 = 3.00$	$t = 5$	$wt = 13.0$
$w5 = 27.44$		L =37.5	

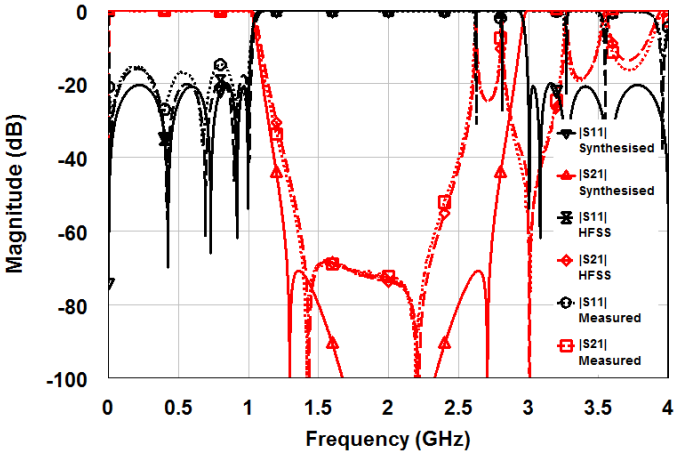

Fig. 12 Comparison of simulated response of the synthesized, HFSS and measurement of meander-like low-pass filter

The low-pass filter is then realised using rectangular bars or striplines. The technique by Getsinger [9, 10] was used to determine the initial physical dimensions. The final optimised dimensions are given in Table VII. The nomenclature used in Table VII corresponds to Fig. 13 and Fig. 14. Fig. 12 shows good correspondence between the measured and theoretical simulation using HFSS.

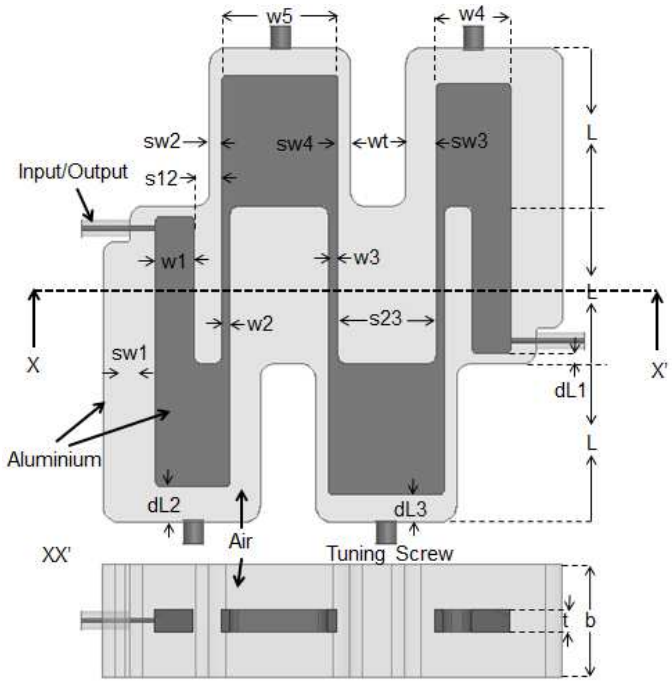

Fig. 13 Diagram showing the layout of the fabricated 9th -degree meander-like low-pass filter. Dimension shown are as given in Table VII

Fig. 14 Physical hardware of the fabricated 9th -degree 'meander-like' low-pass Filter (top cover removed)

The overall length of the low-pass filter realisation is three times the electrical length at the cutoff frequency. High order modes do exist in the structure that potentially could worsen the stopband response especially with relatively larger ground plane spacing. The effect is to shorten the effective stopband frequency window as the design example shows in Fig. 12.

The choice of the ground plane spacing affects the spurious resonances within the filter structure which in this case appeared above $2.6\,GHz$. The insertion loss is fairly low across the passband with a peak at 0.3476 dB at the cutoff frequency in the measured response as depicted in Fig. 15. The slight discrepancy in the insertion loss between the simulated and measurement results in Fig. 15 is due to slight mismatched response as evident from the return loss plot in Fig. 12 and Fig. 16.

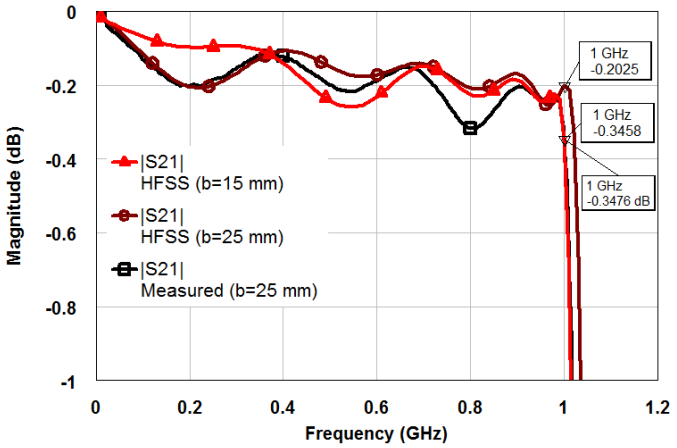

Fig. 15 Comparison of insertion losses between HFSS simulations for b=15 mm and b=25 mm and measured response with b=25 mm.

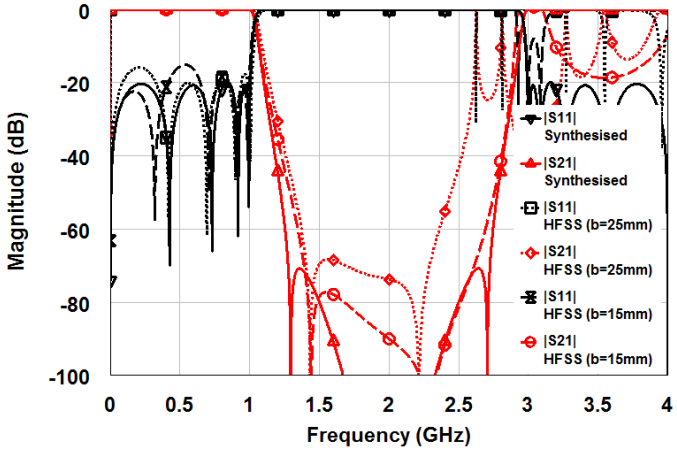

Fig. 16 Comparison of optimised equivalent circuit simulation and HFSS simulations of meander-like low-pass filter with ground plane spacing of 15 mm and 25 mm.

Improvement in the stopband response may be achieved by reducing the ground plane spacing from $b = 25$ mm to $b = 15$ mm at expense of slightly increased insertion loss (Fig. 15). Fig. 16 shows HFSS simulations for different ground plane spacing versus the ideal circuit response. Clearly the stopband performance matches very well with the prediction for $b = 15$ mm. Table VIII shows the corresponding optimized physical dimensions. Notice that much smaller ground plane spacing is limited by realisability of the physical dimensions as the dimensions of the low-pass filter are proportional to the ground plane spacing.

TABLE VIII
IMPROVED 9TH -DEGREE LOW-PASS FILTER OPTIMISED DIMENSIONS (MM)

$w1 = 5.42$	$sw1 = 7.5$	$s12 = 4.80$	$dL1 = 3$
$w2 = 1.11$	$sw2 = 1.8$	$s23 = 13.95$	$dL2 = 5.1$
$w3 = 1.40$	$sw3 = 7.5$	$b = 15$	$dL3 = 3.9$
$w4 = 11.33$	$sw4 = 1.8$	$t = 3$	$wt = 4.65$
$w5 = 16.46$		L =37.5	

C. Comparison

A 9th -degree meander-like low-pass filter was compared to other low-pass filter realisations. To achieve the same selectivity, a 9th -degree generalised Chebyshev low-pass filter would be required while a 15th -degree stepped impedance low-pass filter would be required as depicted in Fig. 17 below with $\pi/4$ electrical length at the cutoff frequency of 1 GHz. Thus for the same selectivity, the proposed structure requires much fewer number of filter elements than the stepped impedance low-pass filter. Although the generalised Chebyshev low-pass filter may be designed with the same degree as the meander-like low-pass filter, its stopband performance is much poorer in its physical realisation as shown in Fig. 17 because the series short circuited stubs are approximated by high impedance transmission lines [3]. Furthermore, both the generalised Chebyshev and stepped impedance low-pass filters' effective stopband response is much worse in practice because it is difficult to realise ideal commensurate transmission line elements and often discontinuities, high order modes and mode conversion occurs within the filter structure [11]. These reduce the effective stopband width of practical low-pass filters to as much as half of the predicted width! Even though effective stopband width may be widened by using a lower electrical length at cutoff frequency, it is often limited by element realisation as the variations in element values tend to be extreme. By utilizing relatively smaller ground plane spacing as described in section B, the proposed low-pass structure offers superior stopband performance.

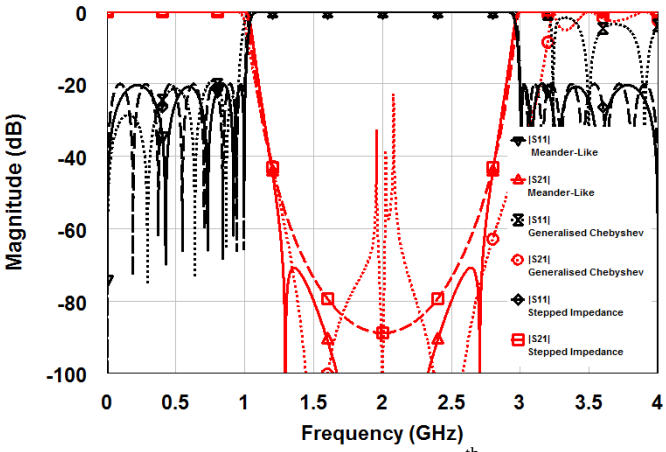

Fig. 17 Circuit simulation comparison of 9th -degree meander-like low-pass filter with a 9th -degree generalised Chebyshev

low-pass filter and 15th -degree stepped impedance low-pass filter.

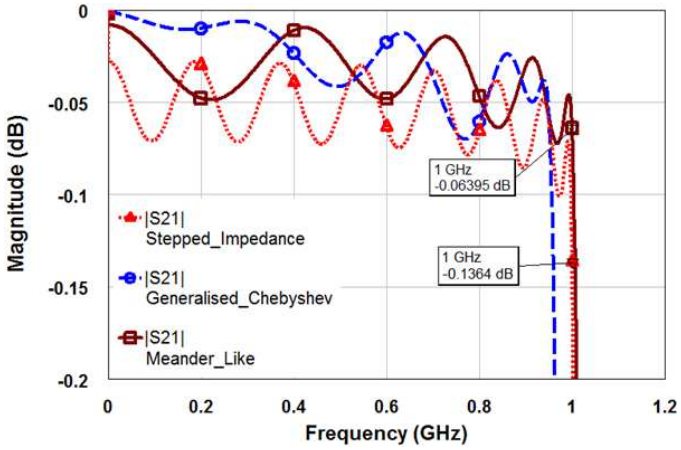

Fig. 18 Circuit insertion loss simulation comparison of 9th -degree meander-like low-pass filter with a 9th -degree generalised Chebyshev low-pass filter and 15th -degree stepped impedance low-pass filter.

Fig. 18 shows the circuit level insertion loss analysis of the three low-pass filters being compared above with the same ground plane spacing of 25 mm assuming copper conductors in air. It is quite obvious the stepped impedance low-pass filter fairs worse because of the highest number of unit elements required to achieve the selectivity. The generalised Chebyshev low-pass filter passband insertion compares well with the proposed meander-like low-pass filter with the losses increasing towards the cutoff frequency. The proposed structure has an optimal number of unit elements equal to the degree of the network regardless of the number finite frequency transmission zeros. The generalised Chebyshev low-pass filter on the other hand requires 12 unit elements to achieve the selectivity requirements. Thus the proposed meander-like low-pass filter is much more compact with low insertion loss than the other two low-pass filters. The meander-like low-pass filter has a high achievable roll-off rate of 246.7 dB/GHz with an achievable relative stopband bandwidth of 0.883 [12] and could be advantageous where a much deeper out-of-band rejection is required.

III. CONCLUSION

An exact design technique for realising generalised Chebyshev distributed low-pass filters using coupled line/stub without approximating the series short circuited stubs has been demonstrated. The physical realisation I has a simple equivalent circuit, however, it requires isolation walls to eliminate coupling between basic sections. Since a single basic section may realise a pair of finite frequency transmission zero, a maximum of $(N-1)/2$ pairs of symmetrically located transmission zeros is achievable. A more general meander-like structure, physical realisation II, with optimal number of elements and simple physical layout of transmission lines has also been presented. Its physical realisation does not require decoupling walls between the parallel coupled line section and hence is easier to construct. However, only certain forms of transfer functions are realisable as described above. Synthesis of a few realisations up to 9th -degree together with the required transmission zeros locations of their canonical forms have been illustrated. A low-pass filter design example utilising the later physical realisation was fabricated and measurement results showed good agreement with theory. Comparison with other low-pass filter realisations reviewed that the proposed low-pass filter has much higher roll-off rate and deeper effective stopband.

REFERENCES

[1] H. M. Jaradat and W. M. Fathelbab, "Selective lowpass filters realizing finite-frequency transmission zeros," in Radio and Wireless Symposium, 2009. RWS '09. IEEE, 2009, pp. 252-255.

[2] C. J. Chen, C. H. Sung, and Y. D. Su, "A Multi-Stub Lowpass Filter," IEEE Microw. Compon. Lett., vol. 25, pp. 532-534, 2015.

[3] I. Hunter, Theory and design of microwave filters: IET, 2001.

[4] J. D. Rhodes and S. Alseyab, "The generalized chebyshev low-pass prototype filter," International Journal of Circuit Theory and Applications, vol. 8, pp. 113-125, 1980.

[5] S. A. Alseyab, "A Novel Class of Generalized Chebyshev Low-Pass Prototype for Suspended Substrate Stripline Filters," IEEE Trans. Microw. Theory Techn., vol. 30, pp. 1341-1347, 1982.

[6] E. Musonda and I. Hunter, "Design of generalised Chebyshev lowpass filters using coupled line/stub sections," in Microwave Symposium (IMS), 2015 IEEE MTT-S International, 2015, pp. 1-4.

[7] R. Sato, "A Design Method for Meander-Line Networks Using Equivalent Circuit Transformations," IEEE Trans. Microw. Theory Techn., vol. 19, pp. 431-442, 1971.

[8] E. Musonda and I. Hunter, "Synthesis of general Chebyshev characteristic function for dual (single) bandpass filters," in Microwave Symposium (IMS), 2015 IEEE MTT-S International, 2015, pp. 1-4.

[9] W. J. Getsinger, "Coupled rectangular bars between parallel plates," IRE Trans. Microw. Theory Techn., vol. 10, pp. 65-72, 1962.

[10] M. A. R. Gunston, Microwave transmission-line impedance data. London Van Nostrand Reinhold, 1972.

[11] R. J. Cameron, C. M. Kudsia, and R. R. Mansour, Microwave filters for communication systems: fundamentals, design, and applications. Hoboken, N.J: Wiley-Interscience, 2007.

[12] J. Wang, L. J. Xu, S. Zhao, Y. X. Guo, and W. Wu, "Compact quasi-elliptic microstrip lowpass filter with wide stopband," Electronics Letters, vol. 46, pp. 1384-1385, 2010.

Evaristo Musonda (GSM'13) received the B.Eng degree (with distinction) from The University of Zambia, Lusaka, Zambia, in 2007, the M.Sc. degree in communication engineering (with distinction) from The University of Leeds, Leeds, U.K., in 2012, and is currently working toward his Ph.D. degree at The University of Leeds. In early 2008 he joined Necor Zambia Limited, an ICT company, before joining the country's largest mobile telecommunication services provider, Airtel Zambia, in June 2008, where he was involved in core network planning, optimization, and support roles for three years. He is currently involved in research for new microwave filters synthesis techniques for digital wireless communication systems at the University of Leeds. His research interests include microwave filters and network synthesis.

Ian Hunter (M'82–SM'94–F'07) received the B.Sc. degree (honors, first class) and Ph.D. degree from Leeds University, Leeds, U.K., in 1978 and 1981, respectively. Early in his career, he was with Aercom, Sunnyvale, CA, USA, and KW Engineering, San Diego, CA, USA, and Filtronic, Shipley, U.K., where he was involved with the development of broadband microwave filters for electronic warfare (EW) applications. From 1995 to 2001, he was with Filtronic Comtek, where he was involved with advanced filters for cellular radio. He currently holds the Royal Academy of Engineering/Radio Design Ltd. Research Chair in Microwave Signal Processing with the School of Electronic and Electrical Engineering, The University of Leeds, Leeds, U.K. He currently leads a team involved with the research of new microwave filters for mobile communications systems. He authored Theory and Design of Microwave Filters (IEE, 2001). Prof. Hunter is a Fellow of the IET and the U.K. Royal Academy of Engineering. He was general chair of 2011 European Microwave Week, Manchester, U.K. He will chair the 2016 European Microwave Conference, London, U.K.